Nonlinear Dyn (2012) 67:2637–2649
DOI 10.1007/s11071-011-0177-1

ORIGINAL PAPER

Supercritical and subcritical Hopf bifurcation and limit cycle oscillations of an airfoil with cubic nonlinearity in supersonic\hypersonic flow

Hulun Guo · Yushu Chen

Received: 4 April 2010 / Accepted: 21 July 2011 / Published online: 31 August 2011

Abstract In this paper, the Hopf bifurcations and limit cycle oscillations (LCOs) of an airfoil with cubic nonlinearity in supersonic\hypersonic flow are investigated. The harmonic balance method and multivariable Floquet theory are applied to analyze the LCOs of the airfoil. Four distinct cases of the LCOs response are detected in this system: (I) supercritical Hopf bifurcation, (II) a single subcritical Hopf bifurcation, (III) two subcritical Hopf bifurcations, and (IV) no Hopf bifurcation. Furthermore, the parameter variations domains separating the supercritical and subcritical Hopf bifurcations are presented using singularity theory.

Keywords Supercritical and subcritical Hopf bifurcation · LCO · Harmonic balance method · Floquet theory · Singularity theory

1 Introduction

Strong interactions may occur between high speed flow fields and aerospace structural components, resulting in several remarkable aeroelastic phenomena. These may dramatically influence the performance of flight vehicles. Moreover, the tendency of the next generation of aeronautical and space vehicles is towards low weight and high structural flexibility [1–3]. However, these will enhance nonlinearities in both structure and aerodynamic loads. Limit cycle oscillations (LCOs) may appear instead of flutter due to such nonlinearities. Properties of a LCO provide important information on the behavior of the aeroelastic system. This can be examined via Hopf bifurcations [4] of the associated nonlinear aeroelastic system [5–7]. Such Hopf bifurcations can be classed as supercritical and subcritical. In the former (benign) case, the LCO appears at speed greater than the flutter speed. In the latter (catastrophic) case, the LCO may appear below the flutter speed [1].

Lee [5] and Dowell [8] have given a detailed review of structural and aerodynamic nonlinearities. Generally, the structural nonlinearity can be described as either cubic, freeplay, or hysteretic. In addition, aerodynamic nonlinearity can have a significant influence on aeroelastic characteristics of the airfoil response in supersonic\hypersonic flow. Such influence can cause catastrophic structural failure. Therefore, the prevention of bifurcation and LCO is an important technology in wing design of flight vehicles.

The first attempt to study nonlinear aeroelasticity was carried out by Woolston et al. [9, 10]. In their work, attention was focused on the hard and soft spring character in a nonlinear two-degree-of-freedom system (2-DOF). They found that the soft spring has a destabilizing effect. Liu and Zhao [11] studied the bifurcations of airfoils in incompressible flow with

H. Guo (✉) · Y. Chen
School of Astronautics, Harbin Institute of Technology, Harbin 150001, China
e-mail: hulunguo@yahoo.cn

nonlinear pitching stiffness by a harmonic balance method, an asymptotic expansion method, an averaging method and a numerical integration method. Lee et al. [12] also came to the same conclusion that the soft spring property destabilizes the subcritical Hopf bifurcation in a 2-DOF airfoil system. The harmonic balance method was also used to investigate the LCOs of a 2-DOF airfoil with cubic nonlinearity in the restoring forces by Lee et al. [13]. They derived analytical expressions for the amplitudes of the pitch and plunge motions. Liu and Dowell [14] used the same method to higher order to study a secondary bifurcation of the airfoil.

The center manifold procedure and normal form theory also play important roles in studying the Hopf bifurcation of a nonlinear system [15]. They were used to study the subcritical and supercritical Hopf bifurcation of a 2-DOF airfoil with structural nonlinearity [16, 17], aerodynamic nonlinearity [18], or time-delay [19]. However, the results obtained by these procedures are satisfactory only in the neighborhood of critical points [20]. Therefore, they are rather limited for an airfoil system.

It should be stressed that the effect of system parameters on Hopf bifurcations and LCOs in an airfoil system with structural and aerodynamic nonlinearities remains unclear. To address this issue, the present investigation focuses on the LCOs of an airfoil in a supersonic\hypersonic flow undergoing Hopf bifurcation. The harmonic balance method and multi-variable Floquet theory are applied to analyze the LCOs of this system. In this paper, a new singularity theory is developed to study the supercritical and subcritical Hopf bifurcations in a structural parameter space.

2 Model equations

We consider the vibration of a 2-DOF plunging/pitching double wedge airfoil as shown in Fig. 1. The nonlinear aeroelastic governing equations can be written as [1–3]:

$$\begin{cases} m\ddot{h} + S_\alpha \ddot{\alpha} + c_h \dot{h} + K_h h = -L, \\ S_\alpha \ddot{h} + I_\alpha \ddot{\alpha} + c_\alpha \dot{\alpha} + K_\alpha \alpha + \hat{K}_\alpha \alpha^3 = M_{\mathrm{EA}}, \end{cases} \tag{1}$$

where h is the plunging displacement (positive downward), α is the pitch angle (positive nose up), superposed dots denote derivatives with respect to time t,

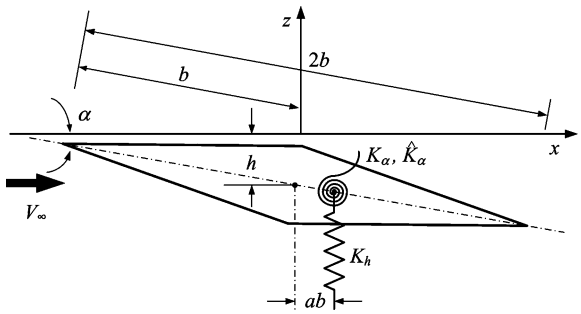

Fig. 1 Two degree-of-freedom airfoil geometry

m is the structural mass per unit span, S_α is the static unbalance about the elastic axis, I_α is the mass moment of inertia about the elastic axis of the airfoil, c_h, c_α, K_h, and K_α are linear viscous damping and stiffness coefficients and $\hat{K}_\alpha$ is the structural nonlinear stiffness coefficient in pitch DOF. The surplus L and M_{EA} denote an unsteady aerodynamic lift and moment respectively. They will be found by the piston theory aerodynamics (PTA) [21]. The PTA is an inviscid unsteady aerodynamic theory, used extensively in the case of supersonic\hypersonic flow ($M_\infty \geq \sqrt{2}$) and for moderate angles ($|\alpha| \leq \pi/6$). It provides a point-function relationship between the local pressure on the surface of the vehicle and the component of fluid velocity normal to the moving surface [22].

In this paper, a third order piston theory is applied. Thus, the unsteady aerodynamic lift L and moment M_{EA} of a 2-DOF plunging/pitching double wedge airfoil are expressed as [23, 24]:

$$\begin{aligned} L = {} & 4p_\infty \gamma M_\infty b\left(\frac{\dot{h}}{V_\infty} - ba\frac{\dot{\alpha}}{V_\infty} + \alpha\right) \\ & - p_\infty \gamma(\gamma+1)M_\infty^2 b^2 \hat{\tau}\left(\frac{\dot{\alpha}}{V_\infty}\right) \\ & + \frac{1}{3}p_\infty \gamma(\gamma+1)M_\infty^3 b \\ & \times \left\{\left(\frac{\dot{h}}{V_\infty} - ba\frac{\dot{\alpha}}{V_\infty} + \alpha\right)\right. \\ & \times \left(\left(\frac{\dot{h}}{V_\infty} - ba\frac{\dot{\alpha}}{V_\infty} + \alpha\right)^2 + 3\hat{\tau}^2\right. \\ & \left.\left. + \left(b\frac{\dot{\alpha}}{V_\infty}\right)^2\right)\right\}, \end{aligned} \tag{2}$$

$$
\begin{aligned}
M_{\mathrm{EA}} &= 4p_\infty \gamma M_\infty b^2 \\
&\quad \times \left(a\frac{\dot h}{V_\infty} - \left(\frac{b}{3} + ba^2\right)\frac{\dot\alpha}{V_\infty} + a\alpha\right) \\
&\quad + p_\infty \gamma(\gamma+1)M_\infty^2 b^2 \hat\tau \\
&\quad \times \left(\frac{\dot h}{V_\infty} - 2ba\frac{\dot\alpha}{V_\infty} + \alpha\right) \\
&\quad - \frac{1}{3}p_\infty \gamma(\gamma+1)M_\infty^3 b^2 \left\{\frac{1}{5}\left(b\frac{\dot\alpha}{V_\infty}\right)^3\right. \\
&\quad - a\left(\frac{\dot h}{V_\infty} - ba\frac{\dot\alpha}{V_\infty} + \alpha\right) \\
&\quad \times \left(\left(\frac{\dot h}{V_\infty} - ba\frac{\dot\alpha}{V_\infty} + \alpha\right)^2 + 3\hat\tau^2\right) \\
&\quad + b\frac{\dot\alpha}{V_\infty}\left(\left(\frac{\dot h}{V_\infty} - ba\frac{\dot\alpha}{V_\infty} + \alpha\right)^2 + \hat\tau^2\right. \\
&\quad \left.\left. - ba\frac{\dot\alpha}{V_\infty}\left(\frac{\dot h}{V_\infty} - ba\frac{\dot\alpha}{V_\infty} + \alpha\right)\right)\right\}. \qquad (3)
\end{aligned}
$$

In addition to the standard parameters that appear in the classical PTA model, $\hat\tau$ here denotes the thickness ratio ($\equiv t_h/b$).

It is convenient to introduce the following dimensionless parameters: $\xi = h/b$, $\tau = V_\infty t/b$, $\chi_\alpha = S_\alpha/(mb)$, $r_\alpha^2 = I_\alpha/(mb^2)$, $\omega_\xi = \sqrt{K_h/m}$, $\omega_\alpha = \sqrt{K_\alpha/I_\alpha}$, $\zeta_\xi = c_h/2(K_h m)^{1/2}$, $\zeta_\alpha = c_\alpha/2(K_\alpha I_\alpha)^{1/2}$, $V^* = V_\infty/(b\omega_\alpha)$, $\bar\omega = \omega_\xi/\omega_\alpha$, $\hat\eta_\alpha = \hat K_\alpha/K_\alpha$, $\mu = m/(4\rho_\infty b^2)$, $p_\infty = \rho_\infty c_\infty^2/\gamma$. In terms of these, the governing equations of a supersonic\hypersonic double wedge airfoil, featuring plunging-pitching coupled motion, can be written:

$$
\begin{cases}
\xi'' + \chi_\alpha \alpha'' + 2\frac{\zeta_\xi \bar\omega}{V^*}\xi' + \frac{\bar\omega^2}{V^{*2}}\xi = -\bar L(\tau), \\
\frac{\chi_\alpha}{r_\alpha^2}\xi'' + \alpha'' + 2\frac{\zeta_\alpha}{V^*}\alpha' + \frac{1}{V^{*2}}(\alpha + \hat\eta_\alpha \alpha^3) \\
\quad = \bar M_{\mathrm{EA}}(\tau),
\end{cases} \qquad (4)
$$

where

$$
\begin{aligned}
\bar L(\tau) &= \frac{1}{12M_\infty\mu}\left\{12(\xi' - a\alpha' + \alpha) - 3(\gamma+1)\hat\tau M_\infty \alpha'\right. \\
&\quad + (\gamma+1)M_\infty^2\left\{(\xi' - a\alpha' + \alpha)\right. \\
&\quad \left.\left.\times\left[(\xi' - a\alpha' + \alpha)^2 + 3\hat\tau^2 + (\alpha')^2\right]\right\}\right\}, \\
\bar M_{\mathrm{EA}}(\tau) &= \frac{1}{12\mu M_\infty r_\alpha^2}\left\{12\left[a\xi' - \left(\frac{1}{3} + a^2\right)\alpha' + a\alpha\right]\right. \\
&\quad + 3(\gamma+1)\hat\tau M_\infty(\xi' - 2a\alpha' + \alpha) \\
&\quad - (\gamma+1)M_\infty^2\left\{\frac{1}{5}(\alpha')^3 - a(\xi' - a\alpha' + \alpha)\right. \\
&\quad \times\left[(\xi' - a\alpha' + \alpha)^2 + 3\hat\tau^2\right] \\
&\quad + \alpha'\left[(\xi' - a\alpha' + \alpha)^2 + \hat\tau^2\right. \\
&\quad \left.\left.\left. - a\alpha'(\xi' - a\alpha' + \alpha)\right]\right\}\right\}.
\end{aligned}
$$

Note that the ratio of the amplitude of α' and α is ω, where ω is a dimensionless frequency. If the frequency of the LCO of the airfoil is $\hat\omega$, then this dimensionless frequency can be written as

$$
\omega = \frac{\hat\omega b}{V_\infty} = \frac{\hat\omega b}{M_\infty c_\infty}. \qquad (5)
$$

From (5), one concludes that ω is a small quantity for supersonic\hypersonic flow. Moreover, the amplitude of ξ' is the same order as the amplitude of α'. Thus higher order (nonlinear) damping, in the aerodynamic lift and moment terms can be omitted resulting in

$$
\begin{aligned}
\bar L(\tau) &= \frac{1}{12M_\infty\mu}\left\{12(\xi' - a\alpha' + \alpha)\right. \\
&\quad - 3(\gamma+1)\hat\tau M_\infty \alpha' + (\gamma+1)M_\infty^2 \\
&\quad \left.\times\left[3\hat\tau^2(\xi' - a\alpha' + \alpha) + \alpha^3\right]\right\}, \\
\bar M_{\mathrm{EA}}(\tau) &= \frac{1}{12\mu M_\infty r_\alpha^2}\left\{12\left[a\xi' - \left(\frac{1}{3} + a^2\right)\alpha' + a\alpha\right]\right. \\
&\quad + 3(\gamma+1)\hat\tau M_\infty(\xi' - 2a\alpha' + \alpha) \\
&\quad - (\gamma+1)M_\infty^2\left[\hat\tau^2\alpha' - 3a\hat\tau^2(\xi' - a\alpha' + \alpha)\right. \\
&\quad \left.\left. - a\alpha^3\right]\right\}.
\end{aligned}
$$

The dimensionless aerodynamic equations take the following form:

$$
\begin{cases}
\hat r\xi'' + N_{11}\xi + N_{12}\xi' + N_{13}\alpha \\
\quad + N_{14}\alpha' + N_{15}\alpha^3 = 0, \\
\hat r\alpha'' + N_{21}\xi + N_{22}\xi' + N_{23}\alpha \\
\quad + N_{24}\alpha' + N_{25}\alpha^3 = 0,
\end{cases} \qquad (6)
$$

where the coefficients $\hat r$ and N_{ij} $(i = 1, 2;\ j = 1, 2, 3, 4, 5)$ are functions of the system parameters and the Mach number given by the expressions in Appendix A.

3 Harmonic balance analysis

The harmonic balance method has been used to study the airfoil system in subsonic flow in the literature [13, 14]. Liu and Zhao [11] have confirmed the usefulness of the harmonic balance method in an airfoil system by comparing with three other methods: the asymptotic expansion method, the averaging method and the numerical integration method. In the following, the harmonic balance method is used to predict the LCOs amplitude of an airfoil in a supersonic\hypersonic flow. Since the aeroelastic model of the airfoil described in (6) is a nonlinear autonomous system, a periodic solution of (6) is assumed to take the form:

$$\begin{aligned}\alpha &= a_0 + a_1\cos\omega\tau,\\ \xi &= b_0 + b_1\cos\omega\tau + b_2\sin\omega\tau\end{aligned} \tag{7}$$

where a_0 and b_0 denote the static equilibrium position in the pitch and plunge DOF respectively and a_1 and $\sqrt{b_1^2+b_2^2}$ denote the amplitude of the LCO in the pitch and plunge DOF, respectively.

Substituting (7) into (6) leads to

$$\begin{aligned}&-\omega^2\hat{r}(b_1\cos\omega\tau + b_2\sin\omega\tau)\\ &\quad + N_{11}(b_0 + b_1\cos\omega\tau + b_2\sin\omega\tau)\\ &\quad - \omega N_{12}(b_1\sin\omega\tau - b_2\cos\omega\tau)\\ &\quad + N_{13}(a_0 + a_1\cos\omega\tau) - N_{14}\omega a_1\sin\omega\tau\\ &\quad + N_{15}\left(a_0^3 + \frac{3}{2}a_0a_1^2\right) + N_{15}\left(3a_0^2a_1 + \frac{3}{4}a_1^3\right)\\ &\quad \times\cos\omega\tau + \text{higher harmonics} = 0,\\ &-\omega^2\hat{r}a_1\cos\omega\tau + N_{21}(b_0 + b_1\cos\omega\tau + b_2\sin\omega\tau)\\ &\quad - \omega N_{22}(b_1\sin\omega\tau - b_2\cos\omega\tau)\\ &\quad + N_{23}(a_0 + a_1\cos\omega\tau) - N_{24}\omega a_1\sin\omega\tau\\ &\quad + N_{25}\left(a_0^3 + \frac{3}{2}a_0a_1^2\right) + N_{25}\left(3a_0^2a_1 + \frac{3}{4}a_1^3\right)\\ &\quad \times\cos\omega\tau + \text{higher harmonics} = 0.\end{aligned} \tag{8}$$

Collecting the constant and the coefficients of $\sin\omega\tau$ and $\cos\omega\tau$, one obtains algebraic equations for a_0, b_0, a_1, b_1, b_2, and ω:

$$N_{11}b_0 + N_{13}a_0 + N_{15}\left(a_0^3 + \frac{3}{2}a_0a_1^2\right) = 0, \tag{9}$$

$$N_{21}b_0 + N_{23}a_0 + N_{25}\left(a_0^3 + \frac{3}{2}a_0a_1^2\right) = 0, \tag{10}$$

$$\omega^2\hat{r}b_2 - N_{11}b_2 + \omega N_{12}b_1 + \omega N_{14}a_1 = 0, \tag{11}$$

$$\omega^2\hat{r}b_1 - N_{11}b_1 - \omega N_{12}b_2 - N_{13}a_1 - 3N_{15}a_0^2a_1 - \frac{3}{4}N_{15}a_1^3 = 0, \tag{12}$$

$$N_{21}b_2 - \omega N_{22}b_1 - \omega N_{24}a_1 = 0, \tag{13}$$

$$\omega^2\hat{r}a_1 - N_{21}b_1 - \omega N_{22}b_2 - N_{23}a_1 - 3N_{25}a_0^2a_1 - \frac{3}{4}N_{25}a_1^3 = 0. \tag{14}$$

In order to solve (9)–(14), the following four cases will be considered: (1) $a_0 = 0$, $a_1 = 0$; (2) $a_0 = 0$, $a_1 \neq 0$; (3) $a_0 \neq 0$, $a_1 = 0$; and (4) $a_0 \neq 0$, $a_1 \neq 0$.

Case (1) $a_0 = 0$, $a_1 = 0$.
This corresponds to the zero solution of (6).

Case (2) $a_0 = 0$, $a_1 \neq 0$.
Substituting $a_0 = 0$ into (12) and (14), yields

$$\omega^2\hat{r}b_1 - N_{11}b_1 - \omega N_{12}b_2 - N_{13}a_1 - \frac{3}{4}N_{15}a_1^3 = 0, \tag{15}$$

$$\omega^2\hat{r}a_1 - N_{21}b_1 - \omega N_{22}b_2 - N_{23}a_1 - \frac{3}{4}N_{25}a_1^3 = 0. \tag{16}$$

Substituting (13) into (11), (15), and (16), and eliminating b_2, gives

$$\begin{aligned}&(\omega^2\hat{r} - N_{11})(N_{22}b_1 + N_{24}a_1)\\ &\quad + N_{21}(N_{12}b_1 + N_{14}a_1) = 0,\end{aligned} \tag{17}$$

$$\begin{aligned}&\left(\omega^2\hat{r}b_1 - N_{11}b_1 - N_{13}a_1 - \frac{3}{4}N_{15}a_1^3\right)N_{21}\\ &\quad - N_{12}\omega^2(N_{22}b_1 + N_{24}a_1) = 0,\end{aligned} \tag{18}$$

$$\begin{aligned}&\left(\omega^2\hat{r}a_1 - N_{21}b_1 - N_{23}a_1 - \frac{3}{4}N_{25}a_1^3\right)N_{21}\\ &\quad - N_{22}\omega^2(N_{22}b_1 + N_{24}a_1) = 0.\end{aligned} \tag{19}$$

Equation (18) and (19) implies:

$$\begin{aligned}&\left(\omega^2\hat{r}b_1 - N_{11}b_1 - N_{13}a_1 - \frac{3}{4}N_{15}a_1^3\right)N_{22}\\ &\quad = \left(\omega^2\hat{r}a_1 - N_{21}b_1 - N_{23}a_1 - \frac{3}{4}N_{25}a_1^3\right)N_{12}.\end{aligned} \tag{20}$$

From (17) and (20), the square dimensionless frequency can be expressed as

$$\omega^2 = \frac{P_2 + P_3 a_1^2}{P_1}. \tag{21}$$

So, (17) and (18) yields

$$P_4\omega^4 + \left(P_5 + P_6 a_1^2\right)\omega^2 + P_7 + P_8 a_1^2 = 0. \tag{22}$$

The expressions for the coefficients P_i $(i = 1, 2, \ldots, 8)$ are given in Appendix B.

Substituting (21) into (22), yields

$$Q_1 a_1^4 + Q_2 a_1^2 + Q_3 = 0, \tag{23}$$

where the expressions for the coefficients Q_i $(i = 1, 2, 3)$ are given in Appendix C.

The flutter Mach number M_F follows from

$$Q_3 = 0. \tag{24}$$

From (23), the amplitude of the LCO in the pitch DOF is obtained as

$$a_1 = \sqrt{\frac{-Q_2 \pm \sqrt{Q_2^2 - 4Q_1Q_3}}{2Q_1}}. \tag{25}$$

Case (3) $a_0 \neq 0$, $a_1 = 0$.
Substituting $a_1 = 0$ into (9) and (10), gives

$$a_0 = \sqrt{N_0}, \tag{26}$$

where $N_0 = \frac{N_{11}N_{23} - N_{13}N_{21}}{N_{15}N_{21} - N_{11}N_{25}}$.

Case (4) $a_0 \neq 0$, $a_1 \neq 0$.
Combining (9) and (10), yields

$$a_0^2 = N_0 - \frac{3}{2}a_1^2. \tag{27}$$

Substituting (27) into (12) and (14), gives

$$\omega^2 \hat{r} b_1 - N_{11}b_1 - \omega N_{12}b_2 - \bar{N}_{13}a_1 - \frac{3}{4}\bar{N}_{15}a_1^3 = 0, \tag{28}$$

$$\omega^2 \hat{r} a_1 - N_{21}b_1 - \omega N_{22}b_2 - \bar{N}_{23}a_1 - \frac{3}{4}\bar{N}_{25}a_1^3 = 0, \tag{29}$$

where $\bar{N}_{13} = N_{13} + 3N_0N_{15}$, $\bar{N}_{23} = N_{23} + 3N_0N_{25}$, $\bar{N}_{15} = -5N_{15}$ and $\bar{N}_{25} = -5N_{25}$.

Similar to case (2), one has

$$\bar{Q}_1 a_1^4 + \bar{Q}_2 a_1^2 + \bar{Q}_3 = 0. \tag{30}$$

And the amplitude of the LCO in the pitch DOF can also be solved from (30). Moreover, $a_0^2 = N_0 - \frac{3}{2}a_1^2 > 0$ should be satisfied.

4 Stability analysis

In terms of $y_1 = \xi$, $y_2 = \xi'$, $y_3 = \alpha$, $y_4 = \alpha'$, $Y = \{y_1, y_2, y_3, y_4\}^T$ (6) can be written as a system of four first-order ordinary differential equations

$$Y' = f(Y), \tag{31}$$

where

$$f(Y) = \frac{1}{\hat{r}}\begin{pmatrix} \hat{r}y_2 \\ -N_{11}y_1 - N_{12}y_2 - N_{13}y_3 - N_{14}y_4 - N_{15}y_3^3 \\ \hat{r}y_4 \\ -N_{21}y_1 - N_{22}y_2 - N_{23}y_3 - N_{24}y_4 - N_{25}y_3^3 \end{pmatrix}. \tag{32}$$

The T-period steady state solution Y_0 of (31) is determined by the solution (7). The parameters in this solution have been determined in the previous section. Thus, Y_0 can be written as

$$Y_0 = \begin{pmatrix} y_1 \\ y_2 \\ y_3 \\ y_4 \end{pmatrix} = \begin{pmatrix} b_0 + b_1\cos\omega\tau + b_2\sin\omega\tau \\ -\omega b_1\sin\omega\tau + \omega b_2\cos\omega\tau \\ a_0 + a_1\cos\omega\tau \\ -\omega a_1\sin\omega\tau \end{pmatrix}. \tag{33}$$

The local stability of Y_0 will be determined by multivariable Floquet theory. Substituting the perturbation solution $Y = Y_0 + \delta Y$ into (31), and ignoring higher order terms in δY, one obtains a linear variational equation with periodic coefficients:

$$\delta Y' = A(\tau)\delta Y, \tag{34}$$

where $A(\tau) = D_Y f(Y_0)$.

In terms of the Jacobian matrix $D_Y f$, the stability of the periodic solution of system (31) is equivalent to the stability of the zero solution of system (34). Furthermore, the stability of the zero solution of system (34) is determined by the transition matrix Φ according to the Floquet theory [25, 26].

Each period $T = \frac{2\pi}{\omega}$ is divided into N intervals. The size of each interval is $\Delta = \frac{T}{N}$, and the kth interval is denoted by $((k-1)\Delta, \Delta)$. In the kth interval

the periodic coefficient matrix $A(\tau)$ can be replaced by a constant matrix B_k defined by

$$B_k = \frac{1}{\Delta}\int_{(k-1)\Delta}^{k\Delta} A(\tau)\,\mathrm{d}\tau = \frac{1}{\hat{r}}\begin{bmatrix} 0 & \hat{r} & 0 & 0 \\ -N_{11} & -N_{12} & -N_{13}-RN_{15} & -N_{14} \\ 0 & 0 & 0 & \hat{r} \\ -N_{21} & -N_{22} & -N_{23}-RN_{25} & -N_{24} \end{bmatrix}, \tag{35}$$

where $R = 3a_0^2 + \frac{3}{2}a_1^2 + \frac{6N}{\pi}a_0a_1 \sin\frac{\pi}{N}\cos(2k-1)\frac{\pi}{N} + \frac{3\pi}{4N}a_1^2 \sin\frac{2\pi}{N}\cos(2k-1)\frac{2\pi}{N}$.

Hence, the approximate transition matrix Φ is given as

$$\Phi = \prod_{i=1}^{N}\left[I + \sum_{j=1}^{N_j}\frac{(\Delta B_i)^j}{j!}\right], \tag{36}$$

where N_j is the number of terms in the approximation of the constant exponential matrix B_i and I is the identity matrix.

The eigenvalues of the monodromy matrix Φ (Floquet multipliers) can be used to determine the stability of a steady state solution. If all eigenvalues have modulus less than unity, the solution is stable. If the modulus of one of the eigenvalues is larger than unity, the solution is unstable.

5 Results analysis

In this section, different LCOs with various system parameters are discussed. The critical Mach number (critical reversal Mach number, flutter Mach number) is also investigated.

The system parameters under consideration are given in Table 1.

In the following numerical simulations, the system parameters listed in Table 1 are fixed, and the remaining parameters $\bar{\omega}$, χ_α, $\hat{\tau}$, and $\hat{\eta}_\alpha$ are varied.

5.1 The critical reversal Mach number analysis

If we take $\bar{\omega} = 1.7$, $\chi_\alpha = 0.25$, $\hat{\tau} = 0.05$, and $\hat{\eta}_\alpha = 50$, the static equilibrium position in pitch DOF a_0 is indicated in Fig. 2. Since $N_0 - \frac{3}{2}a_1^2 < 0$ in case (4), the nonzero solution of a_0 and a_1 does not exist. Therefore, the only solution of a_1 is zero, when a_0 is not

Table 1 System parameters

Parameter	Value	Parameter	Value
r_α	0.5	γ	1.4
ς_ξ, ς_α	0.05, 0.05	μ	100
ω_α	60	c_∞	300 m/s
a	−0.15	b	1 m

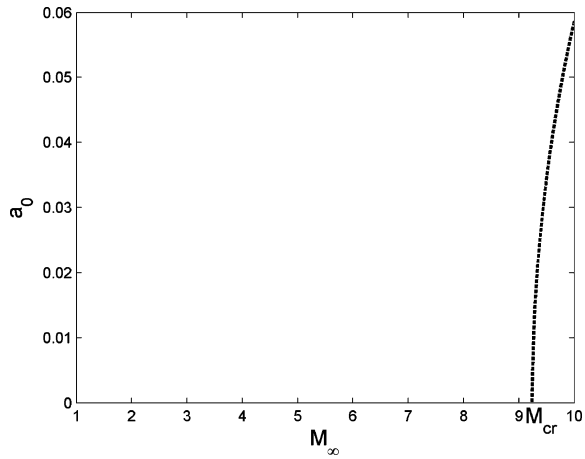

Fig. 2 Static equilibrium position vs. Mach number

equal to zero. Figure 2 shows that a_0 is unstable when $M_\infty > M_{\mathrm{cr}}$ ($M_{\mathrm{cr}} = 9.25$). Hence, there is no stable solution when $M_\infty > M_{\mathrm{cr}}$. Thus, M_{cr} can be defined as a critical reversal Mach number. Furthermore, in order to investigate the LCOs responses, the Mach number should be smaller than the critical reversal Mach number.

From (26), one concludes that the critical reversal Mach number can be solved from

$$N_0 = 0 \tag{37}$$

or

$$\frac{1}{V^{*2}} + \frac{1}{4M_\infty\mu r_\alpha^2}\left[4a + (\gamma+1)\hat{\tau}M_\infty + a(\gamma+1)\hat{\tau}^2M_\infty^2\right] = 0. \tag{38}$$

From (38), one concludes that M_{cr} is independent of $\bar{\omega}$, χ_α, and $\hat{\eta}_\alpha$. From Fig. 3, it follows that M_{cr} decreases as $\hat{\tau}$ increases. Thus, the critical reversal Mach number increases as the thickness of the airfoil decreases.

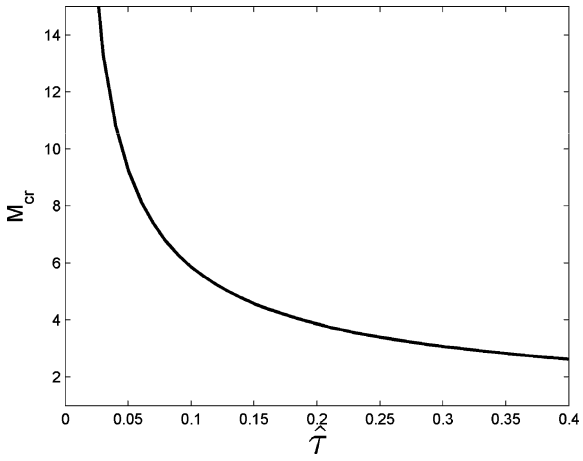

Fig. 3 The critical Mach number vs. the thickness ratio of the airfoil

5.2 LCOs responses analysis

The following study focuses on the cases where $\chi_\alpha = 0.25$, $\hat{\tau} = 0.05$, and $\hat{\eta}_\alpha = 50$, while the value of the frequency ratio $\bar{\omega}$ is taken as 0.8, 1.7, 2.0, and 2.2, respectively. Since the critical reversal Mach number is independent of the frequency ratio, it remains $M_{\text{cr}} = 9.25$ for these four cases. These cases are shown in Fig. 4. They correspond to a supercritical Hopf bifurcation, one subcritical Hopf bifurcation, two subcritical Hopf bifurcations, and no Hopf bifurcation, respectively. The solid curve depicts a stable LCO and the dashed curve depicts an unstable LCO.

The supercritical Hopf bifurcation means that the nonzero solution is on the other side of the stable zero solution in a neighborhood of the Hopf bifurcation. On the other hand, the nonzero solution is on the same side of the stable zero solution, that is corresponding to the subcritical Hopf bifurcation [27, 28].

Figure 4(a) shows that a supercritical Hopf bifurcation exists. There is a stable zero solution for $M_\infty < M_F$ ($M_F = 1.24$). For $M_F < M_\infty < M_{\text{cr}}$, the zero solution becomes unstable, and a stable LCO appears. The LCO amplitude increases as the Mach number increases.

In Fig. 4(b), it can be seen that there is a transition from the supercritical Hopf bifurcation to a subcritical Hopf bifurcation as $\bar{\omega}$ increases. A LCO can appear at $M_L (M_L = 2.79)$, which is smaller than M_F ($M_F = 3.51$). For $M_L < M_\infty < M_F$, there are two LCOs. The one with larger amplitude is stable and the other is unstable. When the disturbance is smaller than the unstable LCO, the dynamic response will stabilize at zero. Otherwise, the response will finally evolve into a stable LCO with large amplitude. This implies that LCO also exists below the flutter Mach number. Such a subcritical Hopf bifurcation is catastrophic for an airfoil.

In Fig. 4(c), there are two Hopf bifurcation points (M_F and M_{F2}), and both of the nonzero solutions are on the same side of the stable zero solutions in the neighborhood of these two Hopf bifurcation points. Thus, these two points are subcritical Hopf bifurcations. From Fig. 4(c), one sees that there is a stable LCO and an unstable zero solution for $M_F < M_\infty < M_{F2}$ ($M_F = 7.13$, $M_{F2} = 7.95$). For $M_{F2} < M_\infty < M_{\text{cr}}$, a new unstable LCO bifurcates from the zero solution, and the zero solution becomes stable.

Figure 4(d) shows an interesting case. For $M_L < M_\infty < M_{\text{cr}}$ ($M_L = 4.21$), there are three solutions, i.e., a stable LCO, an unstable LCO, and a stable zero solution. Moreover, the Hopf bifurcation does not appear below the critical reversal Mach number.

5.3 The flutter Mach number analysis

The flutter Mach number M_F can be solved from (24). Actually, for all the coefficients of (6), $\hat{\eta}_\alpha$ appears only in N_{15} and N_{25}. According to Appendix B, the parameters P_1, P_2, P_4, P_5, and P_7 are independent of $\hat{\eta}_\alpha$. Thus, the parameter Q_3 is also independent of $\hat{\eta}_\alpha$. And the flutter Mach number is independent of $\hat{\eta}_\alpha$.

In the following, various cases are discussed to investigate the effect of the structural parameters $\bar{\omega}$, χ_α, and $\hat{\tau}$ on the flutter Mach number. (See Figs. 5–7.)

For $\chi_\alpha = 0.25$, $\hat{\tau} = 0.05$, and $\hat{\eta}_\alpha = 50$, the $M_F - \bar{\omega}$ curve is shown in Fig. 5. It is shown that the flutter Mach number decreases as the pitch-plunge frequency ratio $\bar{\omega}$ approaches unity. Woolston et al. [9, 10] have drawn a similar conclusion for an airfoil in subsonic flow. To the best of our knowledge, it is unclear in the open literatures what there happens with increasing frequency ratio. In the following, we focus on a detailed answer to this question. From Fig. 5, it can be seen that the flutter Mach number M_F exceeds the critical reversal Mach number for $\bar{\omega} > 2.1$. This implies that a Hopf bifurcation does not exist in cases when the relation between the amplitude of the LCO and Mach number is shown in Fig. 4(d).

For $\bar{\omega} = 1.2$, $\hat{\tau} = 0.05$, and $\hat{\eta}_\alpha = 50$, the $M_F - \chi_\alpha$ curve is shown in Fig. 6. It is seen that the flutter Mach number increases with increasing χ_α.

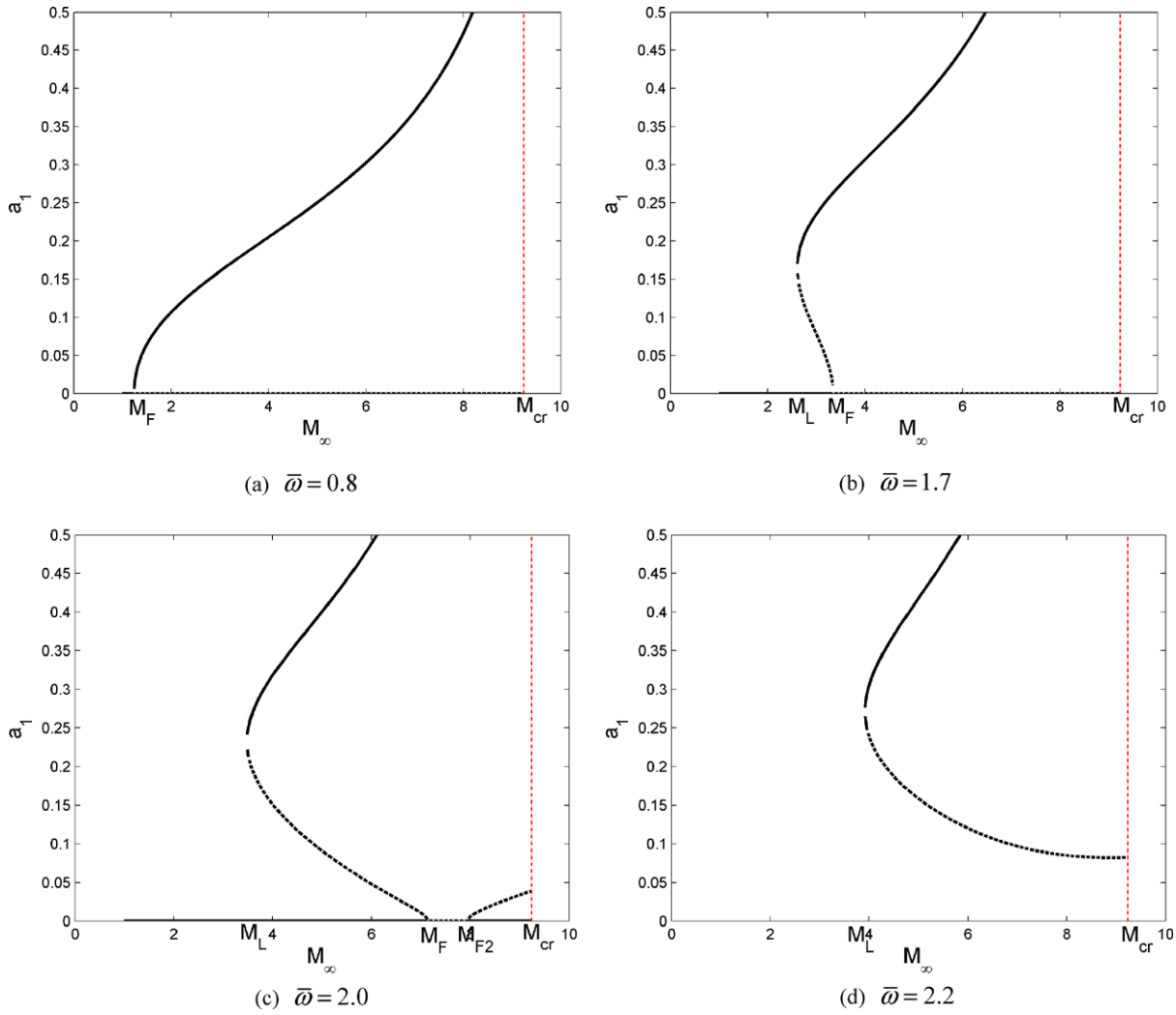

Fig. 4 The LCOs amplitude in pitch vs. Mach number

For $\chi_\alpha = 0.25$, $\bar{\omega} = 1.2$, and $\hat{\eta}_\alpha = 50$, the $M_F - \hat{\tau}$ curve is shown in Fig. 7. It is seen that the flutter Mach number decreases with increasing $\hat{\tau}$. This can be expressed the modern airfoil becoming more and more thin, especially in the supersonic\hypersonic flow.

6 Supercritical and subcritical Hopf bifurcation

Two typical Hopf bifurcations, i.e., supercritical and subcritical Hopf bifurcation, arise in the airfoil system. However, how the structural parameters $\bar{\omega}$, χ_α, $\hat{\tau}$, and $\hat{\eta}_\alpha$ determine these two Hopf bifurcations remains unclear.

Singularity theory offers an extremely useful approach to solve bifurcation problems. It can be used to determine the critical parameter of different types of bifurcations. Golubitsky and Schaeffer [27, 28] gave a detailed introduction of the singularity theory in mathematics. Chen and Leung [15] introduced the singularity theory in simple language, and gave some examples in engineering. In the Mathieu system [29], six typical bifurcations were obtained in the parameter area by singularity theory. In the following, singularity theory is developed to investigate the supercritical Hopf bifurcation and the subcritical Hopf bifurcation of the airfoil system.

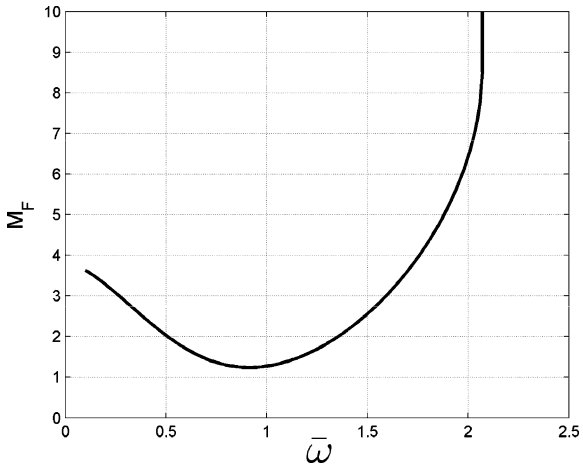

Fig. 5 The flutter Mach number vs. the frequency ratio

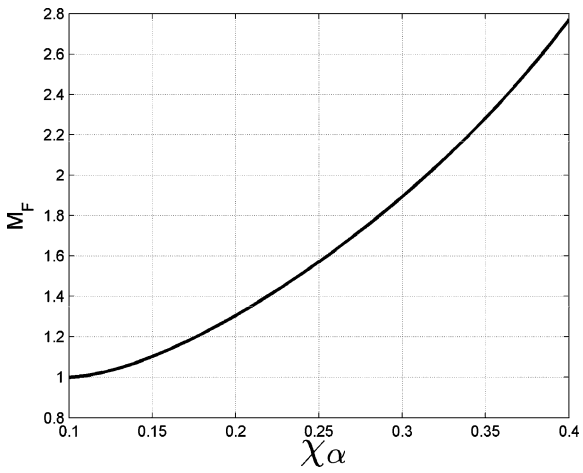

Fig. 6 The flutter Mach number vs. the dimensionless static unbalance

Firstly, the bifurcation equation is introduced as

$$G(a_1, M_\infty, \beta) = Q_1(M_\infty, \beta)a_1^4 + Q_2(M_\infty, \beta)a_1^2 + Q_3(M_\infty, \beta) = 0, \tag{39}$$

where $\beta = \{\chi_\alpha, \bar{\omega}, \hat{\tau}, \hat{\eta}_\alpha\}^T$ is the unfolding parameter.

Figure 8 depicts both a supercritical and subcritical Hopf bifurcation. Point A represents a Hopf bifurcation point, where

$$\frac{\mathrm{d}M_\infty}{\mathrm{d}a_1} = 0. \tag{40}$$

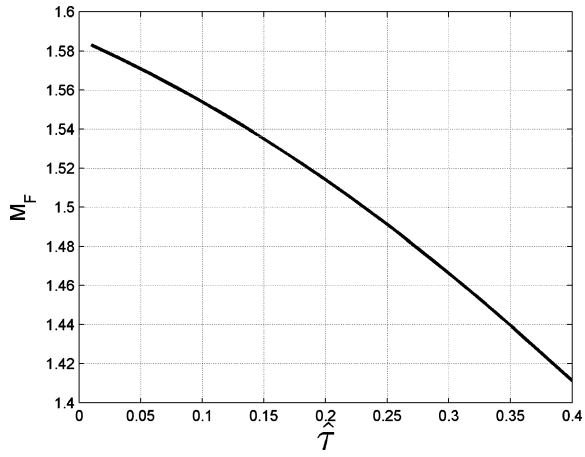

Fig. 7 The flutter Mach number vs. the thickness ratio

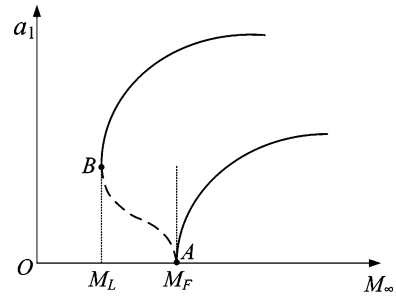

Fig. 8 Supercritical and subcritical Hopf bifurcation

Point B represents an inflection point, where

$$\frac{\mathrm{d}M_\infty}{\mathrm{d}a_1} = 0 \quad \text{and} \quad \frac{\mathrm{d}^2M_\infty}{\mathrm{d}a_1^2} = 0. \tag{41}$$

When point A and point B coincide, i.e., $M_L = M_F$, a small perturbation of the structure parameter will change the nature of the Hopf bifurcation (supercritical Hopf bifurcation or subcritical Hopf bifurcation).

From (39), one has

$$\frac{\mathrm{d}G}{\mathrm{d}a_1} = \frac{\partial G}{\partial a_1} + \frac{\partial G}{\partial M_\infty}\frac{\mathrm{d}M_\infty}{\mathrm{d}a_1} = 0, \tag{42}$$

$$\frac{\mathrm{d}^2G}{\mathrm{d}a_2^2} = \frac{\partial^2 G}{\partial a_2^2} + 2\frac{\partial^2 G}{\partial a_2 \partial M_\infty}\frac{\mathrm{d}M_\infty}{\mathrm{d}a_2} + \frac{\partial G}{\partial M_\infty}\frac{\mathrm{d}^2M_\infty}{\mathrm{d}a_2^2} + \frac{\partial^2 G}{\partial M_\infty^2}\left(\frac{\mathrm{d}M_\infty}{\mathrm{d}a_2}\right)^2 = 0. \tag{43}$$

Then, substituting (39), (40), and (41) into (42) and (43), a simplified critical condition for a supercritical

Hopf bifurcation to convert to a subcritical Hopf bifurcation is obtained:

$$\frac{\partial G}{\partial a_1} = 4Q_1 a_1^3 + 2Q_2 a_1 = 0, \tag{44}$$

$$\frac{\partial^2 G}{\partial a_1^2} = 12Q_1 a_1^2 + 2Q_2 = 0. \tag{45}$$

If $a_1 \neq 0$, M_L can be determined from (39), (44), and (45). In this case, one has

$$\begin{cases} Q_1(M_\infty, \beta) = 0, \\ Q_2(M_\infty, \beta) = 0, \\ Q_3(M_\infty, \beta) = 0. \end{cases} \tag{46}$$

If aerodynamic nonlinearity is neglected, the parameters N_{15} and N_{25} can be expressed as

$$N_{15} = -\chi_\alpha \frac{\hat{\eta}_\alpha}{V^{*2}} \quad \text{and} \quad N_{25} = \frac{\hat{\eta}_\alpha}{V^{*2}}. \tag{47}$$

Then (46) becomes

$$\begin{cases} Q_1(M_\infty, \beta) = \hat{\eta}_\alpha^2 q_1(M_\infty, \beta') = 0, \\ Q_2(M_\infty, \beta) = \hat{\eta}_\alpha q_2(M_\infty, \beta') = 0, \\ Q_3(M_\infty, \beta) = q_3(M_\infty, \beta') = 0, \end{cases} \tag{48}$$

where $\beta' = \{\chi_\alpha, \bar{\omega}, \hat{\tau}\}^T$.

Equation (48) suggests that M_L is independent of $\hat{\eta}_\alpha$. As shown in Fig. 9, the amplitude of the LCOs with different $\hat{\eta}_\alpha$ is obtained, where the aerodynamic nonlinearity is neglected. From Fig. 9, it can be seen that with either a hard spring or a soft spring the LCO amplitude increases with decreasing $|\hat{\eta}_\alpha|$; nevertheless, M_L remains unchanged.

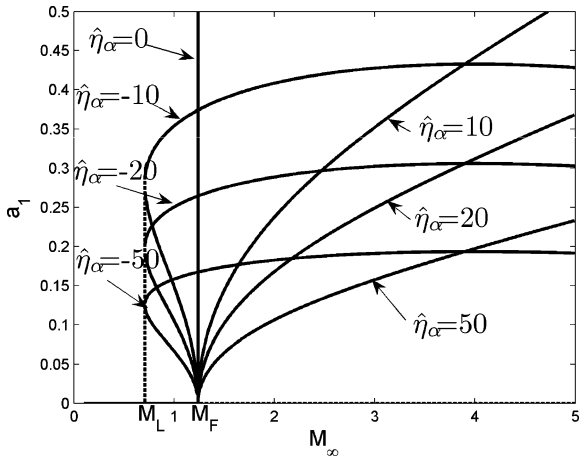

Fig. 9 The LCOs amplitude with different structural nonlinearity

At the Hopf bifurcation point, the amplitude a_1 is 0. In this case, the unfolding parameter β determined by (39), (44), and (45) is defined as the hysteresis set by the singularity theory [15], and the bifurcation diagram of G will change its property under a small perturbation of β. It implies that a supercritical Hopf bifurcation and a subcritical Hopf bifurcation can interchange under a small perturbation of β. According to (39), (44), and (45), the hysteresis set can be expressed as

$$H = \Big\{ \beta \in R^4 | \exists (a_1, M_\infty), \quad \text{s.t. } G = \frac{\partial G}{\partial a_1} = \frac{\partial^2 G}{\partial a_1^2} = 0, \text{ at } a_1 = 0 \Big\}. \tag{49}$$

The flutter Mach number should be lower than the critical reversal Mach number. Thus, (49) can be simplified to

$$H = \big\{ \beta \in R^4 | \exists M_\infty < M_{\text{cr}} \quad \text{s.t. } Q_2(M_\infty, \beta) = Q_3(M_\infty, \beta) = 0 \big\}. \tag{50}$$

Recalling that the unfolding parameter β is composed of $\bar{\omega}$, χ_α, $\hat{\tau}$, and $\hat{\eta}_\alpha$, the hysteresis set can be obtained when two parameters in β are fixed, while the other two vary. Then the parameter domains of the supercritical and subcritical Hopf bifurcation are shown in Fig. 10. Substituting one of the points in the parameter domain into (39), yields a bifurcation diagram where the type of the Hopf bifurcation can be identified. Note that the type of the bifurcation of all the points in one parameter domain is consistent. From Figs. 10(a), (b), and (c), it can be seen how the supercritical and subcritical Hopf bifurcations exchange when the structural nonlinearity is changed.

If aerodynamic nonlinearity is neglected, the hysteresis set can be obtained from

$$\hat{\eta}_\alpha = 0. \tag{51}$$

Equation (51) suggests that the hard spring ($\hat{\eta}_\alpha > 0$) and the soft spring ($\hat{\eta}_\alpha < 0$) represent the supercritical Hopf bifurcation and the subcritical Hopf bifurcation, respectively. This conclusion has also been given in the literature [1, 5]. Note that M_L and M_F are independent of $\hat{\eta}_\alpha$. Thus, neither a hard spring nor a soft

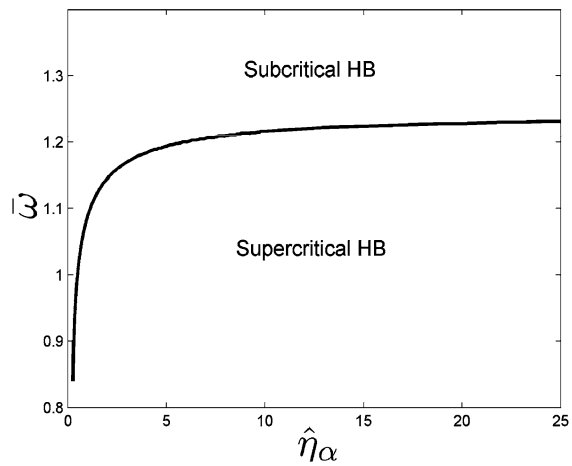

(a) $\chi_\alpha = 0.25,\ \hat{\tau} = 0.05$

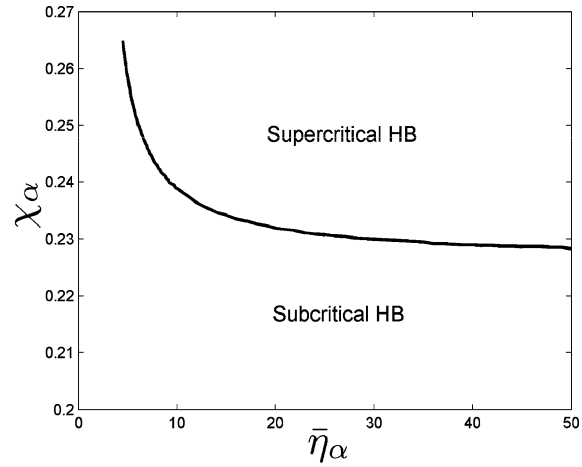

(b) $\bar{\omega} = 1.2,\ \hat{\tau} = 0.05$

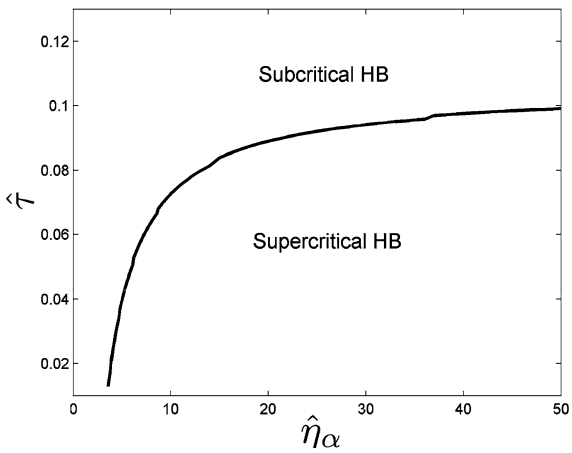

(c) $\bar{\omega} = 1.2,\ \chi_\alpha = 0.25$

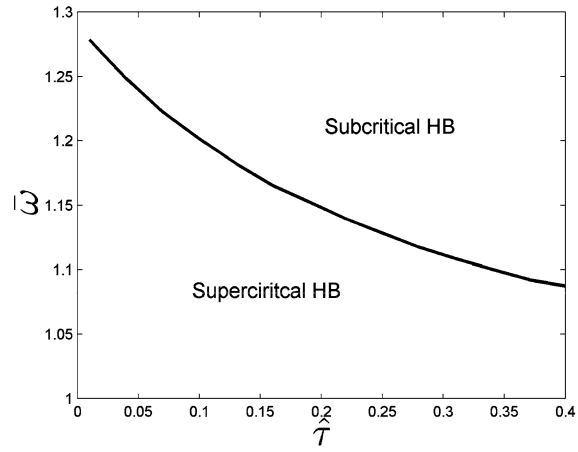

(d) $\chi_\alpha = 0.25,\ \hat{\eta}_\alpha = 50$

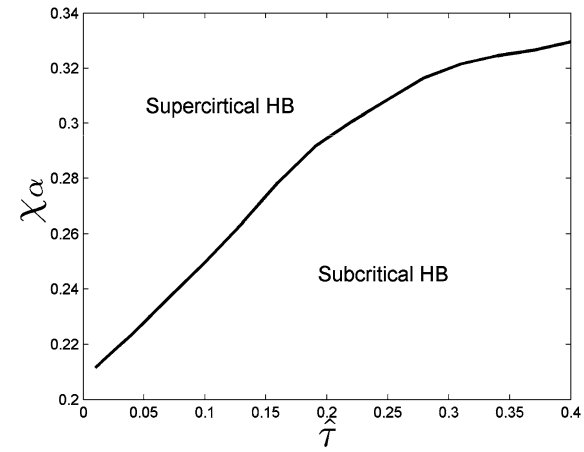

(e) $\bar{\omega} = 1.2,\ \hat{\eta}_\alpha = 50$

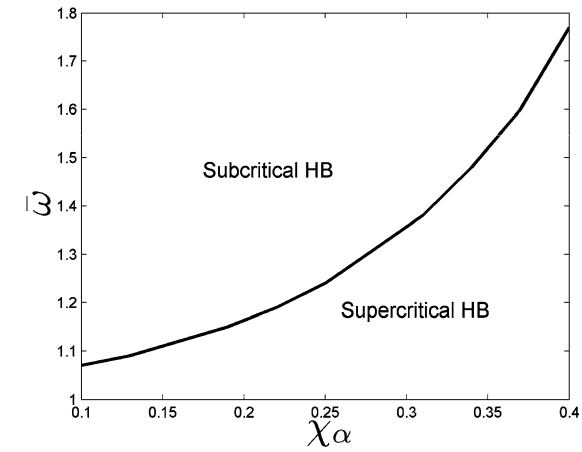

(f) $\hat{\tau} = 0.05,\ \hat{\eta}_\alpha = 50$

Fig. 10 The parameter domains for supercritical and subcritical Hopf bifurcations (HB)

spring $\hat{\eta}_\alpha$ can affect the flutter boundary without aerodynamic nonlinearity. Moreover, from Figs. 10(a), (b), and (c), it is seen that a subcritical Hopf bifurcation can also exist in the hard spring system if aerodynamic nonlinearity is taken into account.

From Figs. 10(a), (d), and (f), it is clear that a subcritical Hopf bifurcation can change to a supercritical Hopf bifurcation as the frequency ratio decreases. From Figs. 10(b), (e), and (f), it is also clear that a subcritical Hopf bifurcation can change to a supercritical Hopf bifurcation as the dimensionless static unbalance increases. Furthermore, from Figs. 10(c), (d), and (e), one sees a subcritical Hopf bifurcation can change to a supercritical Hopf bifurcation as the thickness ratio decreases.

7 Conclusion

In this paper, the LCOs of an airfoil with cubic nonlinearity in a supersonic\hypersonic flow are investigated. The method of multiple scales is applied to the equation of motion to derive approximate solutions of the LCOs. It is shown that a supercritical Hopf bifurcation, a single subcritical Hopf bifurcation, two subcritical Hopf bifurcations, or no Hopf bifurcation occur in this system. It is also proved that the frequency ratio, the static unbalance, and the structural nonlinearity are independent of the critical reversal Mach number. For the supercritical and subcritical Hopf bifurcation, singularity theory is employed as a powerful tool to determine their parameter domains analytically. A subcritical Hopf bifurcation can appear when the airfoil system exhibits a hard spring character, if aerodynamic nonlinearity is taken into account.

Acknowledgements This work is supported by the National Natural Science Foundation of China (Grant Nos. 10632040 and 90816002). The authors gratefully thank Professor R.W. Tucker (Lancaster University) for the assistance in improving the language of the manuscript. The authors are grateful to the anonymous reviewers for their constructive comments and suggestions.

Appendix A: Expressions for the coefficients in (6)

$$\hat{r} = 1 - \frac{\chi_\alpha^2}{r_\alpha^2}, \qquad N_{11} = \left(\frac{\bar{\omega}}{V^*}\right)^2,$$

$$N_{12} = \frac{2\zeta_\xi \bar{\omega}}{V^*} + \frac{1}{4M_\infty \mu r_\alpha^2}\big[\big(r_\alpha^2 + a\chi_\alpha\big) \times \big(4 + (\gamma+1)\hat{\tau}^2 M_\infty^2\big) + \chi_\alpha(\gamma+1)\hat{\tau} M_\infty\big],$$

$$N_{13} = -\frac{\chi_\alpha}{V^{*2}} + \frac{1}{4M_\infty \mu r_\alpha^2}\big[\big(r_\alpha^2 + a\chi_\alpha\big) \times \big(4 + (\gamma+1)\hat{\tau}^2 M_\infty^2\big) + \chi_\alpha(\gamma+1)\hat{\tau} M_\infty\big],$$

$$N_{14} = -\frac{2\chi_\alpha \zeta_\alpha}{V^*} - \frac{1}{12M_\infty \mu r_\alpha^2} \times \big[3\big(r_\alpha^2 + 2a\chi_\alpha\big)(\gamma+1)\hat{\tau} M_\infty + \big(\chi_\alpha + 3ar_\alpha^2 + 3\chi_\alpha a^2\big)\big(4 + (\gamma+1)\hat{\tau}^2 M_\infty^2\big)\big],$$

$$N_{21} = -\frac{\chi_\alpha}{r_\alpha^2}\left(\frac{\bar{\omega}}{V^*}\right)^2,$$

$$N_{22} = -\frac{2\zeta_\xi \chi_\alpha \bar{\omega}}{r_\alpha^2 V^*} - \frac{1}{4M_\infty \mu r_\alpha^2} \times \big[(\chi_\alpha + a)\big(4 + (\gamma+1)\hat{\tau}^2 M_\infty^2\big) + (\gamma+1)\hat{\tau} M_\infty\big],$$

$$N_{23} = \frac{1}{V^{*2}} - \frac{1}{4M_\infty \mu r_\alpha^2} \times \big[(\chi_\alpha + a)\big(4 + (\gamma+1)\hat{\tau}^2 M_\infty^2\big) + (\gamma+1)\hat{\tau} M_\infty\big],$$

$$N_{24} = \frac{2\zeta_\alpha}{V^*} + \frac{1}{12M_\infty \mu r_\alpha^2}\big[3(2a + \chi_\alpha)(\gamma+1)\hat{\tau} M_\infty + \big(1 + 3a\chi_\alpha + 3a^2\big)\big(4 + (\gamma+1)\hat{\tau}^2 M_\infty^2\big)\big],$$

$$N_{15} = -\chi_\alpha \frac{\hat{\eta}_\alpha}{V^{*2}} + \frac{(\gamma+1)M_\infty}{12\mu r_\alpha^2}\big(r_\alpha^2 + a\chi_\alpha\big),$$

$$N_{25} = \frac{\hat{\eta}_\alpha}{V^{*2}} - \frac{(\gamma+1)M_\infty}{12\mu r_\alpha^2}(a + \chi_\alpha).$$

Appendix B: Expressions for the coefficients in (21) and (22)

$$P_1 = \hat{r}(N_{24} + N_{12}),$$

$$P_2 = N_{11}N_{24} + N_{23}N_{12} - N_{21}N_{14} - N_{22}N_{13},$$

$$P_3 = \frac{3}{4}(N_{12}N_{25} - N_{22}N_{15}),$$

$$P_4 = \hat{r}^2 N_{24},$$

$$P_5 = N_{12}(N_{12}N_{24} - N_{14}N_{22} + \hat{r}(N_{21}N_{14} + N_{22}N_{13} - 2N_{11}N_{24}),$$

$$P_6 = \frac{3}{4}\hat{r}N_{22}N_{15},$$
$$P_7 = N_{11}(N_{11}N_{24} - N_{14}N_{21}) + N_{13}(N_{12}N_{21} - N_{11}N_{22}),$$
$$P_8 = \frac{3}{4}N_{15}(N_{12}N_{21} - N_{11}N_{22}).$$

Appendix C: Expressions for the coefficients in (23)

$$Q_1 = P_1P_3P_6 + P_3^2P_4,$$
$$Q_2 = P_1^2P_8 + P_1P_2P_6 + P_1P_3P_5 + 2P_2P_3P_4,$$
$$Q_3 = P_1^2P_7 + P_1P_2P_5 + P_2^2P_4.$$

References

1. Librescu, L., Chiocchia, G., Marzocca, P.: Implications of cubic physical/aerodynamic nonlinearities on the character of the flutter instability boundary. Int. J. Non-Linear Mech. **38**(2), 173–199 (2003)
2. Librescu, L., Na, S., Marzocca, P., Chung, C.: Active aeroelastic control of 2-D wing-flap systems in an incompressible flow field. AIAA Paper 2003-1414 (2003)
3. Abbas, L.K., Qian, C., Marzocca, P., Zafer, G., Mostafa, A.: Active aerothermoelastic control of hypersonic double-wedge lifting surface. Chin. J. Aeronaut. **21**, 8–18 (2008)
4. Hopf, E.: Bifurcation of a periodic solution from a stationary solution of a system of differential equations. Berl. Math. Phys. Klasse, Sachsischen. Akad. Wiss. Leip. **94**, 3–32 (1942)
5. Lee, B.H.K., Price, S.J., Wong, Y.S.: Nonlinear aeroelastic analysis of airfoils: bifurcation and chaos. Prog. Aerosp. Sci. **35**, 205–334 (1999)
6. Holmes, P.J.: Bifurcations to divergence and flutter in flow-induced oscillations: a finite-dimensional analysis. J. Sound Vib. **53**(4), 471–503 (1977)
7. Mastroddi, F., Morino, L.: Limit-cycle taming by nonlinear control with application to flutter. Aeronaut. J. **100**(999), 389–396 (1996)
8. Dowell, E., John, E., Thomas, S.: Nonlinear aeroelasticity. J. Aircr. **40**(5), 857–874 (2003)
9. Woolston, D.S., Runyan, H.L., Byrdsong, T.A.: Some effects of system nonlinearities in the problem of aircraft flutter. NACA TN 3539 (1995)
10. Woolston, D.S., Runyan, H.L., Andrews, R.E.: An investigation of effects of certain types of structural nonlinearities on wing and control surface flutter. J. Aeronaut. Sci. **24**, 57–63 (1957)
11. Liu, J.K., Zhao, L.C.: Bifurcation analysis of airfoils in incompressible flow. J. Sound Vib. **154**(1), 117–124 (1992)
12. Lee, B.H.K., Jiang, L.Y., Wong, Y.S.: Flutter of an airfoil with a cubic restoring force. J. Fluids Struct. **13**, 75–101 (1999)
13. Lee, B.H.K., Liu, L., Chung, K.W.: Airfoil motion in subsonic flow with strong cubic nonlinear restoring forces. J. Sound Vib. **281**, 699–717 (2005)
14. Liu, L., Dowell, E.H.: The secondary bifurcation of an aeroelastic airfoil motion: effect of high harmonics. Nonlinear Dyn. **37**(1), 31–49 (2004)
15. Chen, Y.S., Leung, A.Y.T.: Bifurcation and Chaos in Engineering. Springer, London (1998)
16. Liu, L., Wong, Y.S., Lee, B.H.K.: Application of the centre manifold theory in non-linear aeroelasticity. J. Sound Vib. **234**(4), 641–659 (2000)
17. Coller, B.D., Chamara, P.A.: Structural non-linearities and the nature of the classic flutter instability. J. Sound Vib. **277**, 711–739 (2004)
18. Ding, Q., Wang, D.L.: The flutter of an airfoil with cubic structural and aerodynamic non-linearities. Aerosp. Sci. Technol. **10**, 427–434 (2006)
19. Yu, P., Chen, Z., Librescu, L., Marzocca, P.: Implications of time-delayed feedback control on limit cycle oscillation of a two-dimensional supersonic lifting surface. J. Sound Vib. **304**, 974–986 (2007)
20. Shahrzad, P., Mahzoon, M.: Limit cycle flutter of airfoils in steady and unsteady flows. J. Sound Vib. **256**(2), 213–225 (2002)
21. Ashley, H., Zartarian, G.: Piston theory—a new aerodynamic tool for the aeroelastician. J. Aeronaut. Sci. **23**(12), 1109–1118 (1956)
22. Abbas, L.K., Chen, Q., O'Donnell, K., Valentine, D., Marzocca, P.: Numerical studies of a non-linear aeroelastic system with plunging and pitching freeplays in supersonic/hypersonic regimes. Aerosp. Sci. Technol. **11**, 405–418 (2007)
23. Thuruthimattam, B.J., Friedmann, P.P., McNamara, J.J., Powell, K.G.: Modeling approaches to hypersonic aeroelasticity. ASME International Mechanical Engineering Congress and Exposition, 2002–32943 (2001)
24. Friedmann, P.P., McNamara, J.J., Thuruthimattam, B.J., Nydick, I.: Aeroelastic analysis of hypersonic vehicles. J. Fluids Struct. **19**, 681–712 (2004)
25. Friedmann, P., Hammond, C.E., Woo, T.H.: Efficient numerical treatment of periodic systems with application to stability problems. Int. J. Numer. Methods Eng. **11**, 1117–1136 (1977)
26. Ge, Z.M., Chen, H.H.: Bifurcations and chaotic motions in a rate gyro with a sinusoidal velocity about the spin axis. J. Sound Vib. **200**(2), 121–137 (1997)
27. Golubitsky, M., Schaeffer, D.G.: Singularities and Groups in Bifurcation Theory, vol. 1. Springer, New York (1985)
28. Golubitsky, M., Schaeffer, D.G.: Singularities and Groups in Bifurcation Theory, vol. 2. Springer, New York (1988)
29. Chen, Y.S., Langford, W.F.: The subharmonic bifurcation solution of nonlinear Mathieu's equation and Euler dynamically buckling problem. Acta Mech. Sin. **20**, 522–532 (1988)